[CANCER RESEARCH 64, 6652–6659, September 15, 2004]

A Unique Structure for Epidermal Growth Factor Receptor Bound to GW572016 (Lapatinib): Relationships among Protein Conformation, Inhibitor Off-Rate, and Receptor Activity in Tumor Cells

Edgar R. Wood,[2] Anne T. Truesdale,[2] Octerloney B. McDonald,[2] Derek Yuan,[2] Anne Hassell,[1] Scott H. Dickerson,[1] Byron Ellis,[3] Christopher Pennisi,[3] Earnest Horne,[3] Karen Lackey,[4] Krystal J. Alligood,[5] David W. Rusnak,[5] Tona M. Gilmer,[5] and Lisa Shewchuk[1]

[1]Departments of Computational, Analytical and Structural Sciences, [2]Assay Development and Compound Profiling, [3]Gene Expression and Protein Biochemistry, [4]High-Throughput Chemistry, and [5]Oncology Biology, GlaxoSmithKline, Inc., Research Triangle Park, North Carolina

ABSTRACT

GW572016 (Lapatinib) is a tyrosine kinase inhibitor in clinical development for cancer that is a potent dual inhibitor of epidermal growth factor receptor (EGFR, ErbB-1) and ErbB-2. We determined the crystal structure of EGFR bound to GW572016. The compound is bound to an inactive-like conformation of EGFR that is very different from the active-like structure bound by the selective EGFR inhibitor OSI-774 (Tarceva) described previously. Surprisingly, we found that GW572016 has a very slow off-rate from the purified intracellular domains of EGFR and ErbB-2 compared with OSI-774 and another EGFR selective inhibitor, ZD-1839 (Iressa). Treatment of tumor cells with these inhibitors results in down-regulation of receptor tyrosine phosphorylation. We evaluated the duration of the drug effect after washing away free compound and found that the rate of recovery of receptor phosphorylation in the tumor cells reflected the inhibitor off-rate from the purified intracellular domain. The slow off-rate of GW572016 correlates with a prolonged down-regulation of receptor tyrosine phosphorylation in tumor cells. The differences in the off-rates of these drugs and the ability of GW572016 to inhibit ErbB-2 can be explained by the enzyme-inhibitor structures.

INTRODUCTION

Several new cancer therapies are being developed that target the ErbB receptor tyrosine kinase family. The receptors are multidomain proteins that contain an extracellular ligand binding domain, a single transmembrane domain, and an intracellular tyrosine kinase domain. The family has three catalytically active members, epidermal growth factor receptor (EGFR; ErbB-1), ErbB-2, and ErbB-4. A fourth member of the family, ErbB-3, does not have tyrosine kinase activity but retains ligand-binding function and is competent for signal transduction (1).

Inhibition of the tyrosine kinase activity of these receptors is one approach for therapeutic intervention (2, 3). At least four ErbB-targeted tyrosine kinase inhibitors are currently in Phase II clinical trials or beyond. These include ZD-1839 (Iressa), OSI-774 (Tarceva), GW572016 (Lapatinib), and CI-1033 (3). These compounds share a common 4-anilinoquinazoline core, but they have distinct ErbB inhibition profiles and mechanisms of action. ZD-1839 and OSI-774 are potent, selective inhibitors of EGFR (4, 5). GW572016 is a potent inhibitor of both EGFR and ErbB-2 (6, 7). CI-1033 was designed to covalently modify an active site cysteine from a template with high initial binding affinity for EGFR. ErbB-2 and ErbB-4 contain the same active site Cys, so CI-1033 inhibits these receptors as well (8).

GW572016 is a potent inhibitor of purified EGFR and ErbB-2 receptor tyrosine phosphorylation in intact cells and ErbB-driven tumor growth in tissue culture and animal models (7). The compound was selected for drug discovery progression because of these and other desirable properties. During the discovery phase of the GW572016 program, we evaluated many different substituted quinazoline compounds and found that potent inhibition of purified receptors was not enough to guarantee potent inhibition in intact cells (7, 9–11). In this report we present a detailed evaluation of inhibitor potency, ErbB receptor selectivity, and inhibitor-enzyme dissociation rate in an effort to better understand the biological activity of molecules in this series. We find that GW572016 has a unique mechanism of action. It exhibits reversible, noncovalent inhibition of EGFR and ErbB-2, but it has a very slow off-rate compared with other reversible 4-anilinoquinazoline compounds.

The crystal structures of apo-EGFR and EGFR bound to OSI-774 (OSI-774/EGFR) were described recently (12). The EGFR structure reveals key features associated with EGFR regulation and catalytic activity. The OSI-774/EGFR structure provides the basic binding mode of the 4-anilinoquinazoline core and identifies key interactions that provide potency and selectivity for EGFR inhibition. The reasons for the slow off-rate for GW572016 relative to other 4-anilinoquinazoline inhibitors is not readily apparent from the compound structure or models based on the OSI-774/EGFR protein structure. For this reason we determined that the crystal structure of EGFR bound to GW572016 (GW572016/EGFR). GW572016/EGFR has a significantly different structure than OSI-774/EGFR. The potential relationship between this novel EGFR structure and the off-rates for 4-anilinoquinazoline inhibitors are discussed. Moreover, the structure may help shed light on previously unexplained aspects of ErbB receptor activation and selectivity of 4-anilinoquinazoline inhibitors.

The dissociation rate of the inhibitor-receptor complex or overall enzyme receptor structure may impact the potency or duration of receptor inhibition in biological models. Down-regulation of receptor autophosphorylation in tumor cell lines is a reliable measure of ErbB inhibitor action. We evaluated the recovery of receptor tyrosine phosphorylation in tumor cells after washing away free compound. Receptor phosphorylation after treatment with GW572016 recovers very slowly in a manner that reflects the dissociation rate of the inhibitor from the purified enzyme.

MATERIALS AND METHODS

Compound Synthesis. Compounds were synthesized and purified according to the published procedures, including GW572016 (6), OSI-774 (13), ZD-1839 (14), and CI-1033 (8).

Enzyme Assays and Data Analysis. We have described previously the purification, general assay methods, and substrate kinetic constants for EGFR, ErbB-2, and ErbB-4 intracellular domains (15). In the experiments presented herein, we measured phosphorylation of the ErbB substrate peptide [Biotin-(amino hexanoic acid)–RAHEEIYHFFFAKKK- $CONH_2$] using the homogeneous time-resolved fluorescence procedure. The concentration of peptide was

Received 4/3/04; revised 7/6/04; accepted 7/13/04.

The costs of publication of this article were defrayed in part by the payment of page charges. This article must therefore be hereby marked *advertisement* in accordance with 18 U.S.C. Section 1734 solely to indicate this fact.

Requests for reprints: Edgar R. Wood, Department of Assay Development and Compound Profiling, GlaxoSmithKline, Inc., Research Triangle Park, NC 27709-13398. Phone: 919-483-3910; Fax: 919-483-3895; E-mail: erw39216@gsk.com.

0.8 μmol/L, and the concentration of ATP was 10 μmol/L unless otherwise indicated.

To measure the IC_{50} for enzyme inhibition, the indicated compound was serially diluted 1 to 3 in dimethyl sulfoxide and added to the reactions to produce an 11-point dose-response curve ranging from 0.00005 to 5 μmol/L. The IC_{50} values were estimated from data fit to Equation A:

$$y = V_{max}\{1 - [x/(K + x)]\} + y_2 \quad (A)$$

V_{max} is the curve fit parameter that represents the upper asymptote of the dose response. This value is typically equivalent to the level of product formed in the absence of inhibitor. x is the variable representing the concentration of inhibitor. K is the curve fit parameter for the IC_{50} value. This occurs at the inflection point of the dose response. y_2 is the curve fit parameter that represents the lower asymptote of the dose response. For a potent inhibitor, y_2 is equivalent to the assay baseline (signal in the absence of enzyme activity).

For K_i^{app} determinations, IC_{50}s were obtained for each compound using eight different concentrations of ATP in the enzyme assay, 10, 40, 70, 100, 130, 160, 190, and 220 μmol/L. Within an experiment each IC_{50} was determined in triplicate. Three independent experiments were performed, and the average IC_{50} was plotted as a function of the concentration ATP. The inhibitors that we have evaluated have been determined previously to be competitive with ATP. Therefore, the Ki^{app} values were obtained from a least squares fit of the data to Equation B (16):

$$IC_{50} = K_i^{app}(1 + [ATP]/K_m^{ATP}) + E/2 \quad (B)$$

E is the curve fit parameter that represents the concentration of enzyme in the reaction. This parameter was constrained to a value <2 nM. Two nM is the maximum concentration of enzyme based on the estimate of total protein in the preparation. The parameter value for E was allowed to float, because the precise concentration of enzyme capable of binding each compound is not known. For all of the K_i^{app} estimates described in Table 1, E was estimated to be at or very near 1 nM. The value of K_m^{ATP} was fixed to 5 μmol/L for EGFR and 30 μmol/L for ErbB-2 based on our experimental values determined previously (15). Calculated K_i^{app} values (cK_i^{app}) were determined for compounds with IC_{50}s >1 μm. These values were obtained by determining IC_{50} at a single concentration of ATP (20 μmol/L) and calculated using Equation B.

Table 1 *ErbB enzyme inhibition by compounds in clinical development*

Compound	EGFR	ErbB-2	ErbB-4
GW572016	[a] = K_i^{app}, [b] = IC_{50}, [c] = cK_i^{app} (nM)		
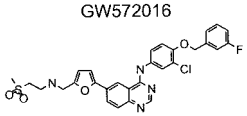			
ZD 1839	3.0 ± 0.2[a]	13 ± 1[a]	347 ± 16[c]
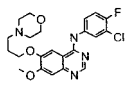			
OSI-774	0.40 ± 0.1[a]	870 ± 90[a]	1130 ± 370[c]
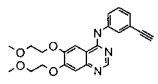			
CI-1033	0.7 ± 0.1[a]	1000 ± 100[a]	1530 ± 270[c]
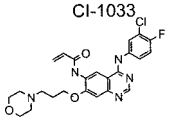			
	30 ± 20[b]	127 ± 42[b]	388 ± 174[b]

NOTE. The method for enzyme assays, experimental design for potency estimation, and data analysis procedures were conducted as described in Materials and Methods. The estimates of inhibitor affinity differ according to the mode of inhibition and potency of the particular result. K_i^{app} values were determined to assess tight-binding inhibition (IC_{50} < 500 nM). Calculated K_i^{app} values (cK_i^{app}) are given for inhibition that yielded an initial IC_{50} > 1,000 nM. CI-1033 is a covalent modifier, so K_i^{app} values are not appropriate measures of potency. For this compound the nonprocessed assay IC_{50} values are given. For K_i^{app} values, the standard error of the least squares fit of the data is shown. For IC_{50} and cK_i^{app} values, the SD of the mean determined from three independent experiments is shown.

We evaluated the recovery of enzyme activity from a preformed enzyme–inhibitor complex to estimate inhibitor off-rate. Enzyme and inhibitor, 500 nM each, were incubated together in 50 mmol/L 4-morpholinepropanesulfonic acid (pH 7.5) and 0.01% Tween for 30 minutes at ambient temperature. This complex was diluted 1:1,000 into standard enzyme assay mixtures containing 200 μmol/L ATP. The reaction was allowed to proceed for the indicated time, and the phosphorylated peptide product was measured. The data were fit to Equation C (17):

$$P = v_s t + [(v_r - v_s)/k_{obs}][1 - \exp(-k_{obs}t)] \quad (C)$$

The value k_{obs} represents the rate of change from v_r (velocity at t = 0) to v_s (velocity upon equilibrium). Using these reaction conditions, essentially 100% of the enzyme is bound by inhibitor in the preformed complex such that $v_r = 0$. Upon reaching equilibrium, the total inhibitor concentration is 0.5 nM. The concentration of ATP is 40 × K_m^{ATP} so that at equilibrium, all of the free enzyme is essentially occupied by ATP, and v_s = 100% of control reactions run in the absence of inhibitor. To be sure that these conditions hold true, control reactions with inhibitor added to the reaction mix (0.5 nM) without being preincubated with enzyme were conducted, and the rate was the same as the rate in the absence of inhibitor.

For all of the data analysis described above, nonlinear regressions were conducted using the program Sigma Plot (Jandel Scientific, San Rafael, CA).

Cell Culture and Treatment. The source and culture conditions of the LICR-LON-HN5 cell line (HN5) have been described previously (7). Cells were subcultured in 150-cm^2 flasks before use. Cells were plated at a density of 250,000 cells per 100 × 20-mm dish on day 1. On day 4, cells were exposed to growth medium containing 0.1% DMSO (vehicle) or to medium containing vehicle and GW572016, OSI-774, or ZD-1839 at 1 μmol/L for 4 hours. Cells were rinsed twice with growth medium and were maintained in fresh growth medium for 0 to 96 hours. After 0, 24, 48, 72, and 96 hours after removal of compounds, cells were rinsed with cold PBS and were lysed on ice with 0.5 mL of cold radioimmunoprecipitation assay buffer + [150 mmol/L NaCl, 50 mmol/L Tris-HCl (pH 7.5), 0.25% deoxycholate, 1% NP40, protease inhibitor mixture, and 1 mmol/L sodium orthovanadate].

SDS-PAGE and Western Blot Analysis. EGFR was immunoprecipitated from 0.1 mg of lysate using 1 μg of anti-EGFR Ab-13 (Lab Vision, Fremont, CA). Immune complexes were precipitated with 50 μL of Protein G Plus/Protein A agarose (Calbiochem, San Diego, CA). Bead pellets were resuspended in 50 μL of 1× Novex Tris-Glycine SDS sample buffer (Invitrogen, Carlsbad, CA) containing 0.25% β-mercaptoethanol. Samples were boiled, and 20 μL were loaded on duplicate 6% Novex Tris-Glycine gels (Invitrogen). Gels were transferred to nitrocellulose, and membranes were blocked in Tris-buffered saline-Tween [150 mmol/L NaCl, 10 mmol/L Tris-HCl (pH 7.5), and 0.1% Tween 20] containing 4% bovine serum albumin. Phosphotyrosine was detected using clone PT66 (Sigma, St. Louis, MO) diluted 1:1,000 in blocking buffer. EGFR was detected using anti-EGFR Ab-12 (Lab Vision) diluted 1:2,500 in blocking buffer. Horseradish peroxidase-conjugated donkey antimouse IgG (Jackson ImmunoResearch Laboratories, Inc., West Grove, PA) was diluted 1:10,000 in blocking buffer, and bands were visualized using enhanced chemiluminescence (Amersham, Piscataway, NJ). Films were scanned using a Fluor S Multi-Imager (Bio-Rad, Hercules, CA), and bands were quantified by densitometry. The ratio of phosphorylated receptor to total receptor was calculated for each sample and was expressed as a percentage of the vehicle-treated control.

Crystallization and Structure Determination. EGFR, residues 672 to 998, was expressed and purified as described previously (12). EGFR was concentrated to 3–5 mg/mL in 50 mmol/L Tris (pH 8.0) and 100 mmol/L NaCl. The protein was complexed with a 3-fold molar excess of GW572016 and incubated on ice for 1 hour. Crystals were grown by the hanging drop vapor diffusion method from 100 mmol/L 3-(cyclohexylamino)propanesulfonic acid (pH 9.0), 200 mmol/L $LiSO_4$, and 2 mol/L $NaKPO_4$ at 22°C. Crystals typically appeared in 2 to 5 days and were harvested and flash frozen in paraffin oil. Data were collected at beam line 17ID on an ADSC detector and processed with HKL0 (18). Crystals belonged to the space group $P2_12_12_1$ with cell dimensions a = 45.65, b = 67.14, c = 102.88, $\alpha = \beta = \gamma = 90$, and 1 mol/asu. The structure was solved by molecular replacement using CNX (19) and PDB-1M14 as the starting coordinates. The structure was rebuilt using QUANTA (Accelrys, San Diego, CA) and refined to an Rfactor of 20% at 2.4Å

using CNX. The R_{merge} and completeness of the data were 6.7% and 95%, respectively. The root mean squared deviation in the bonds and angles of the final model were 0.007Å and 1.30°, respectively.

RESULTS

Potency and Selectivity of 4-Anilinoquinazoline ErbB Inhibitors. Different laboratories have used different methods to evaluate the potency and selectivity of the 4-anilinoquinazoline ErbB inhibitors in clinical development. Potency and selectivity measurements can be affected by experimental conditions, especially enzyme and substrate concentrations and incubation times. To provide directly comparable estimates of potency and selectivity, we evaluated enzyme inhibition using a purified enzyme assay system consisting of the recombinant human intracellular domain of each catalytically active ErbB family member (15).

The dissociation constant for an inhibitor, K_i, is the best standard of comparison for potency and selectivity. We estimated K_i^{app} (K_i determined at a single fixed concentration of peptide) by measuring the initial rate of product formation at varied inhibitor concentrations using eight fixed concentrations of ATP. All of the 4-anilinoquinazoline inhibitors being evaluated are potent inhibitors of EGFR with reported IC_{50} values close to the concentration of enzyme normally required to achieve an adequate assay signal (4–8). Therefore, the data were fit to Equation B, which takes into account the concentration of active enzyme in the assay. This allowed us to estimate K_i^{app} values below the enzyme concentration limit (16). We determined the K_i^{app} for EGFR using ZD-1839 and GW572016 (Fig. 1). The IC_{50} value for each compound increased with increasing ATP concentration as expected for a competitive inhibitor. The K_i^{app} values were estimated from the slopes of the lines formed by fitting the data to Equation B. Similar experiments were conducted with ZD-1839, OSI-774, and GW572016 using EGFR, ErbB-2, and ErbB-4 (Table 1). The K_i^{app} values for EGFR that we obtained using ZD-1839 and OSI-774 were 0.4 and 0.7 nM, respectively. These values are lower than the previously reported K_i values of 2.1 ± 0.2 nM for ZD-1839 (4) and 2.7 nM for OSI-774 (5). The inclusion of the enzyme concentration term in our analysis may contribute to these observed differences. ZD-1839 and OSI-774 are both >1,000-fold selective for EGFR over ErbB-2 with K_i^{app} values near 1 μmol/L for ErbB-2.

CI-1033 is an irreversible inhibitor that inactivates ErbB family enzymes by covalently modifying an active site cysteine (8). For compounds of this sort, K_i^{app} estimates as determined in these studies are not appropriate evaluations of binding potency. Nevertheless, we measured the IC_{50} of CI-1033 for EGFR, ErbB-2, and ErbB-4 after 20 minutes of incubation time to estimate the affinity of this compound for the different ErbB enzymes. CI-1033 is a potent pan-ErbB inhibitor that inhibits EGFR, ErbB-2, and ErbB-4 with IC_{50} values of 30, 127, and 388 nM, respectively.

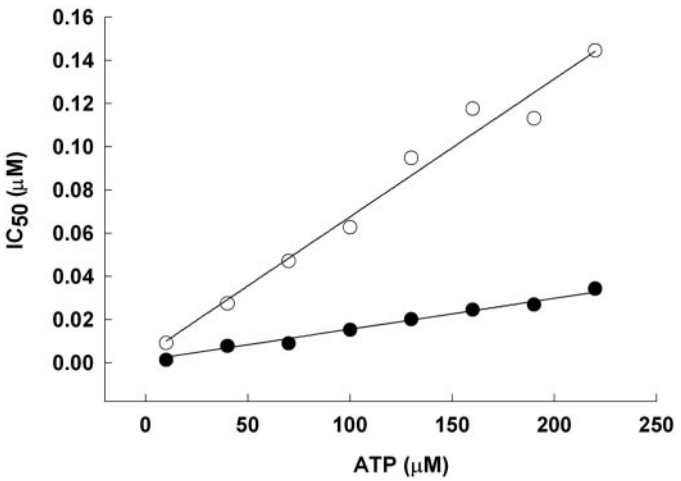

Fig. 1. Determination of K_i^{app} for ZD-1839 and GW572016. The IC_{50} for EGFR with the indicated compound was determined at eight fixed concentrations of ATP. EGFR IC_{50} with ZD-1839 (●). EGFR IC_{50} with GW572016 (○). *Lines* represents the least squares fit of the data to Equation B. The parameters for K_i^{app} from this and other experiments are summarized in Table 1.

GW572016 is unique among the molecules studied, because it is a reversible inhibitor that is potent against both EGFR and ErbB-2 with estimated K_i^{app} values of 3 nM and 13 nM, respectively.

Inhibitor Dissociation Rates. Preliminary evaluation of IC_{50} as a function of time suggested that GW572016 exhibited time-dependent behavior. To characterize this behavior further, we evaluated the inhibitor off-rate using an enzyme reactivation procedure. EGFR and inhibitor were incubated for 30 minutes to allow formation of an enzyme-inhibitor complex. This complex was diluted extensively into a reaction mixture containing a high concentration of ATP ($40 \times K_m$), and phosphorylated product was evaluated as a function of time (Fig. 2). Under these conditions, the change in the rate of product formation reflects the dissociation of the enzyme–inhibitor complex (17). Dissociation of ZD-1839, OSI-774, and GW572016 were compared (Fig. 2*A*). The rates of product formation in the presence of ZD-1839 and OSI-774 were virtually indistinguishable from the rate of product formation in the absence of inhibitor. This indicates a rapid off-rate (half-life < 10 min). In contrast, enzyme activity after preincubation with GW572016 recovered very slowly suggesting that the compound had a much slower off-rate.

To estimate this slow off-rate, we compared GW572016 to the covalent modifier CI-1033 and ran the reactions for a longer period of time (Fig. 2*B*). No recovery of enzyme activity was seen after preincubation with CI-1033. In contrast, phosphorylated product was detected 50 minutes after dilution of the EGFR-GW572016 complex. The off-rate estimated from the fit of data to Equation C is 0.0023 ± 0.0002 per minute. This translates to a half-life of 300 minutes for the GW572016-EGFR complex. GW572016 is a potent inhibitor of EGFR and ErbB-2, so we compared the dissociation of the compound from both enzymes (Fig. 2*C*). GW572016 also has a very slow off-rate for ErbB-2.

The slow recovery of enzyme activity indicates that GW572016 binds in a reversible fashion. Because the recovery was slow, however, we evaluated whether or not GW572016 forms a stable covalent bond with EGFR using liquid chromatography-mass spectrometry. EGFR that was incubated with CI-1033 had a molecular weight consistent with the formation of a single modified cysteine residue as reported previously for a closely related compound (20). EGFR incubated with GW572016 had a molecular weight identical to that of untreated EGFR, which indicated that a stable covalent bond was not formed between the protein and compound (data not shown).

Duration of Inhibition in Tumor Cells. Exposure to kinase inhibitors causes the down-regulation of tyrosine phosphorylation of ErbB receptors in tumor cells (4, 5, 7). We examined the recovery of receptor phosphorylation after inhibitor washout to determine whether there is a correlation between inhibitor dissociation rate and recovery of autophosphorylation (Fig. 3). Logarithmically growing HN5 cells that naturally overexpress EGFR (21) were treated for 4 hours with GW572016, OSI-774, and ZD-1839 (1 μmol/L). After treatment, the inhibitor containing media was removed, cells were rinsed extensively, and fresh media without inhibitor was added. The cells were lysed at various times after inhibitor washout, and EGFR was captured by immunoprecipitation. The relative receptor content was determined by immunoblot with a separate antireceptor antibody, and the state of phosphorylation was analyzed by immunoblot with an antiphospho-

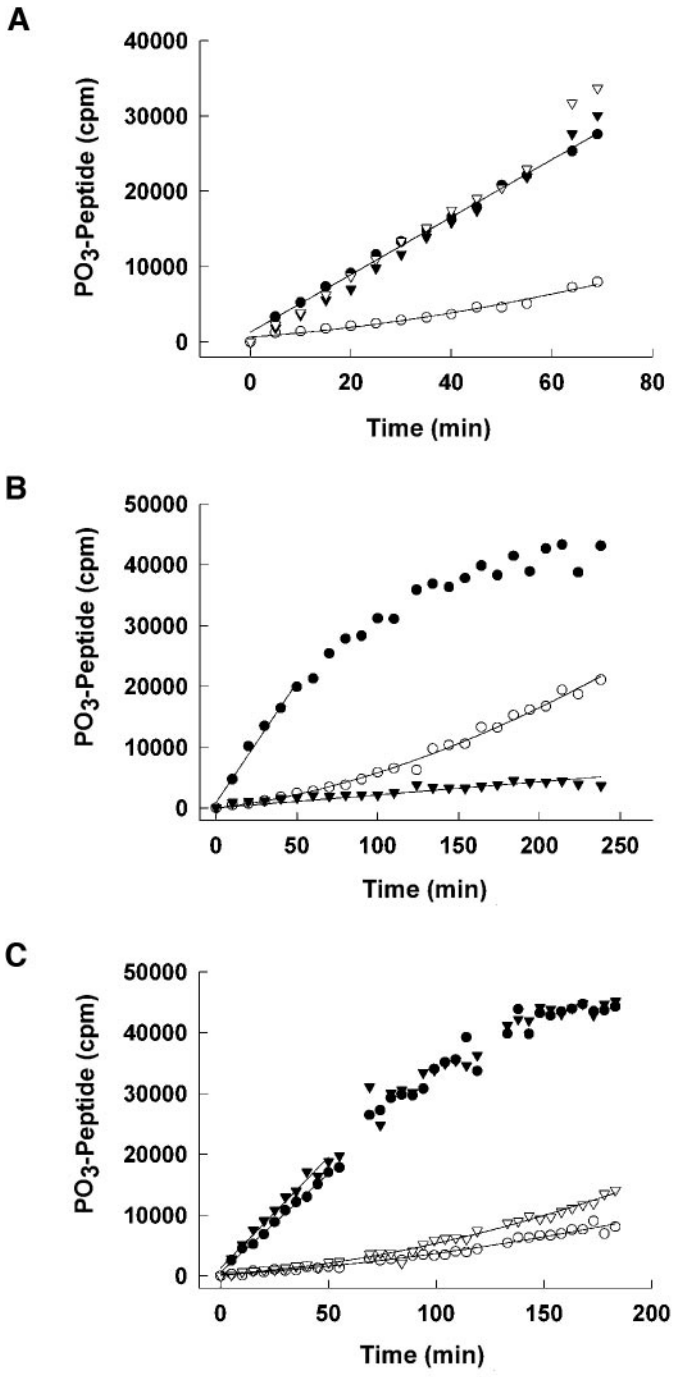

Fig. 2. Dissociation of 4-Anilinoquinazoline Compounds from EGFR and ErbB-2. Phosphorylation of peptide substrate as a function of time is shown. The reaction was initiated by diluting a preformed enzyme-inhibitor complex into reaction buffer. Under the conditions of the reaction, the recovery of activity reflects the dissociation of inhibitor to generate the active enzyme species. Lines represent the least squares fit of the data to equation 3. *A*, Phosphorylation of peptide by EGFR after preincubation with no inhibitor (●), GW572016 (○), OSI-774 (▼), and ZD-1839 (▽). *B*, phosphorylation of peptide by EGFR after preincubation with no inhibitor (●), GW572016 (○), and CI-1033 (▼). *C*, phosphorylation of peptide by EGFR or ErbB-2 after preincubation with GW572016. ErbB-2 with no inhibitor (●), ErbB-2 with GW5720106 (○), EGFR with no inhibitor (▼), and EGFR with GW572016 (▽).

tyrosine antibody. Treatment with all three of the inhibitors resulted in >85% reduction in receptor tyrosine phosphorylation without any reduction in total receptor content. In OSI-774-treated cells, receptor phosphorylation recovered to control levels 24 hours after washout. In ZD-1839-treated cells, recovery of receptor phosphorylation was slower but had reached 60% of control levels after 72 hours. Receptor phosphorylation in GW572016-treated cells had only recovered to 15% of control levels 96 hours after washout. These results suggest that the very slow inhibitor dissociation rate of GW572016 may increase the duration of suppression of ErbB receptor activity in tumor cells.

Crystal Structure of GW572016/EGFR. The dramatic differences between the off-rates observed for GW572016 and OSI-774 suggested that the two compounds were binding to EGFR in different ways. To test this hypothesis, we evaluated the binding mode of GW572016 by determining the crystal structure of EGFR bound to the inhibitor. The structure of GW572016/EGFR was solved to 2.4 Å resolution and contains the kinase domain, as well as 40 residues of the COOH-terminal tail. The overall fold of the protein is similar to that observed in apo-EGFR and OSI-774/EGFR structures (12). However, there are significant differences in the orientation of the NH_2- and COOH-terminal lobes, the COOH-terminal tail, and the C helix, as described below. Six residues at the NH_2 terminus, 8 residues at the COOH-terminus, and five short loop regions (residues 710 to 713, 726 to 730, 844 to 851, 964 to 970, and 980 to 983) are not included in the final model due to poor electron density.

Inhibitor Binding Site. GW572016 binds in the ATP-binding cleft in a fashion similar to that observed in other kinase-quinazoline

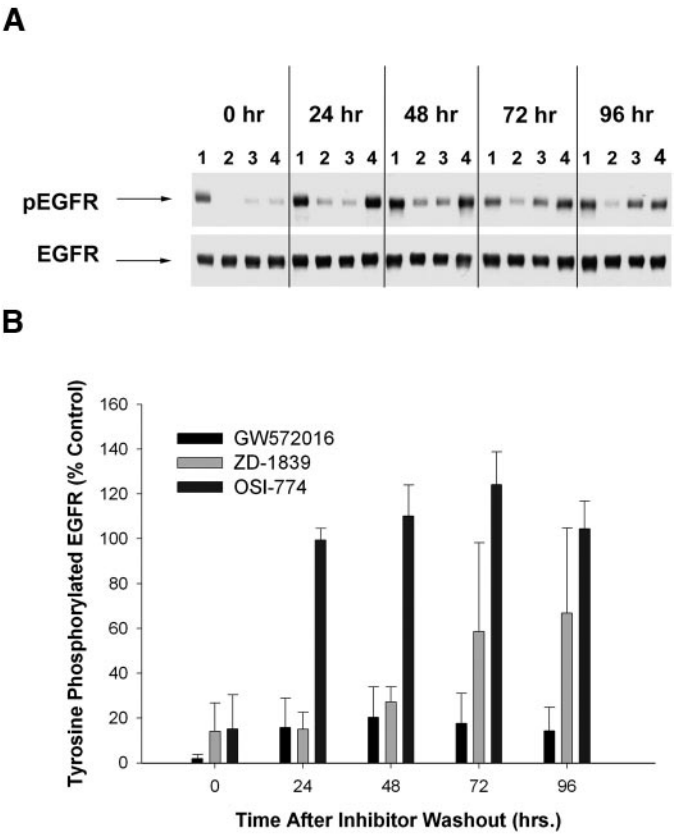

Fig. 3. Recovery of EGFR autophosphorylation after treatment with GW572016, ZD-1839, and OSI-774. Logarithmically growing HN5 cells were treated with 1 μmol/L inhibitor in culture media for 4 hours. The media was removed, cells were washed twice, and fresh compound-free media was added. The cells were lysed at the indicated time after inhibitor washout, and EGFR was isolated by immunoprecipitation. *A*, tyrosine phosphorylated EGFR (*pEGFR*) was determined by Western blot using antiphosphotyrosine antibody. Lysates used for immunoprecipitation were prepared from cells treated with the following agent: *Lane 1*, DMSO control; *Lane 2*, GW572016; *Lane 3*, ZD-1839; and *Lane 4*, OSI-774. Total EGFR was measured from the same immunoprecipitate samples by Western blot using anti-EGFR antibody. *B*, The level of Tyrosine-phosphorylated EGFR was quantified for each condition and expressed as the percentage of vehicle-treated sample. The results represent the mean value of three independent experiments; *bars*, ±SD.

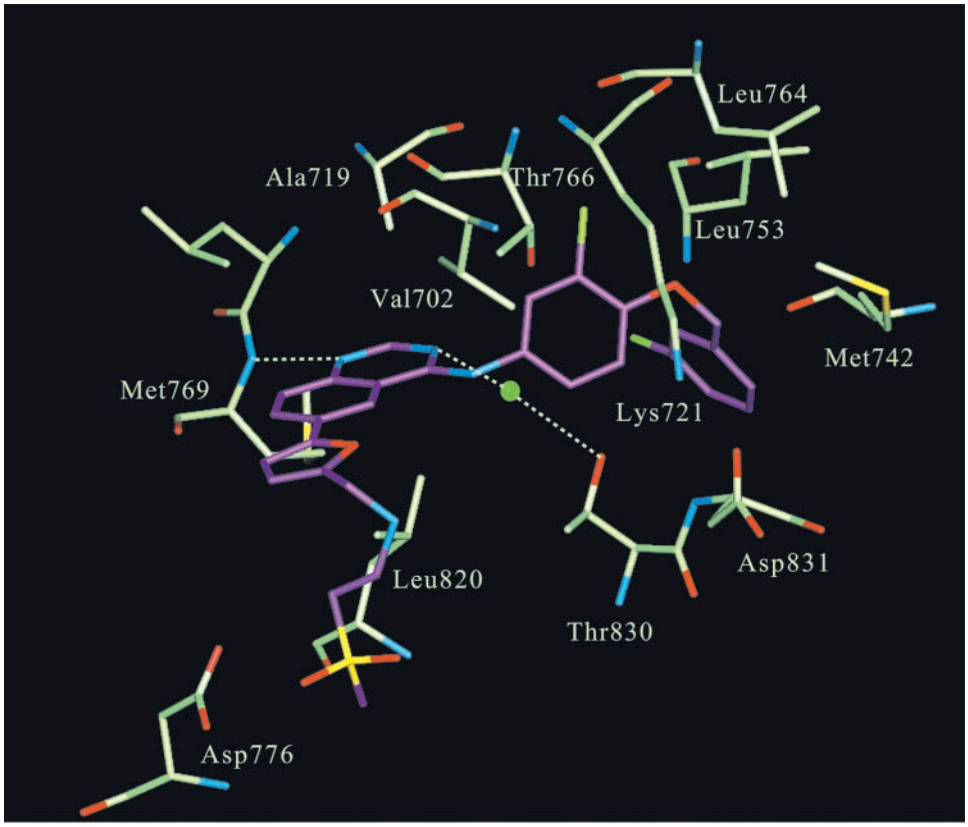

Fig. 4. GW572016 in the ATP binding site of EGFR. GW572016 is shown in *purple*. Hydrogen bonds are indicated by *dashed lines*. The figure was prepared using QUANTA (Accelrys).

crystal structures (refs. 12, 22; Fig. 4). The quinazoline ring is hydrogen bonded to the hinge region between the NH_2- and COOH-terminal lobes of the kinase. N1 of the quinazoline is hydrogen bonded to the main chain NH of Met769, whereas N3 makes a water-mediated hydrogen bond to the side chain of Thr830. The quinazoline ring is sandwiched from the top and bottom by the side chains of Ala719 and Leu820, respectively. The 3′-chloro-4′-[(3-fluorobenzyl)oxy]aniline group is oriented deep in the back of the ATP binding site and makes predominantly hydrophobic interactions with the protein. The 3′-chloro-aniline group is positioned in a pocket formed by the side chains of Val702, Lys721, Leu764, Thr766, Thr830, and Asp831. The 3-fluorobenzyloxy group occupies a pocket formed by the side chains of Met742, Leu753, Thr766, Thr830, Phe832, and Leu834. The aniline nitrogen and the ether oxygen are not involved in any direct hydrogen bonding interactions with the protein. The methylsulfonylethylaminomethylfuryl group, off the C6 position of the quinazoline, is positioned at the solvent interface and does not make any significant interactions with the protein. The methylsulfonylethylamino group is bound near Asp776 but is poorly defined.

Comparison with OSI-774/EGFR. The structure of GW572016/EGFR is very different from the structure of OSI-774/EGFR. These differences include the shape of the ATP binding site, the position of the C helix, the conformations of the COOH-terminal tail and activation loop, and the hydrogen bonding pattern with the quinazoline ring of the inhibitors.

The NH_2- and COOH-terminal lobes of kinases are connected by a flexible hinge region. The relative orientation of the two lobes with respect to one another influences the shape of the ATP binding cleft and is dependent on the activation state of the kinase and the presence of ligands. The ATP binding cleft of GW572016/EGFR is in a relatively closed conformation. This conformation is similar to the ATP binding clefts in inactive Src and Hck (23–25). The ATP binding cleft in OSI-774/EGFR is in a more open conformation. The NH_2-terminal lobe in EGFR/GW572016 is rotated ~12° relative to its position in EGFR/OSI-774 (Fig. 5).

The ATP binding site of GW572016/EGFR has a larger back pocket than apo-EGFR or OSI-774/EGFR. The larger pocket is created by an ~9 Å shift in one end of the C helix to accommodate the 3-fluorobenzyl-oxy group of GW572016 (Fig. 6). The 3-fluorobenzyl-oxy group occupies roughly the same space as Met742 in the C helix of EGFR/OSI-774. The shift in the C helix results in the loss of a highly conserved Glu-Lys salt bridge (Glu738 and Lys721) that ligates the phosphate groups of ATP. In GW572016/EGFR, Lys721 is hydrogen bonded to the side chain of Asp831, located in the COOH-terminal lobe, and Glu738 points out toward solvent.

The COOH-terminal tail of EGFR contains several sites of autophosphorylation and plays a key role in signal transduction by serving as a docking site for signaling molecules that bind to the phosphorylated tyrosines. Forty residues of the COOH-terminal tail were included in the EGFR constructs used in these crystallographic studies. In apo-EGFR and OSI-774/EGFR, the COOH terminus is poorly defined and is loosely associated with two symmetry-related molecules. In GW572016/EGFR, residues 971 to 980 of the COOH-terminal tail form a short α helix that packs along the hinge region connecting the NH_2- and COOH-terminal lobes (Fig. 5). This helix partially blocks the front of the ATP binding cleft. A second helical segment containing residues 983 to 990 extends along the NH_2-terminal lobe of the protein.

Protein kinases contain a large flexible loop, called the activation loop or A-loop that regulates kinase activity (26, 27). Apo-EGFR and OSI-774/EGFR have A-loop conformations (residues 831 to 860) that are similar to A-loops found in active kinase structures. GW572016/EGFR has an A-loop conformation similar to that observed in crystal

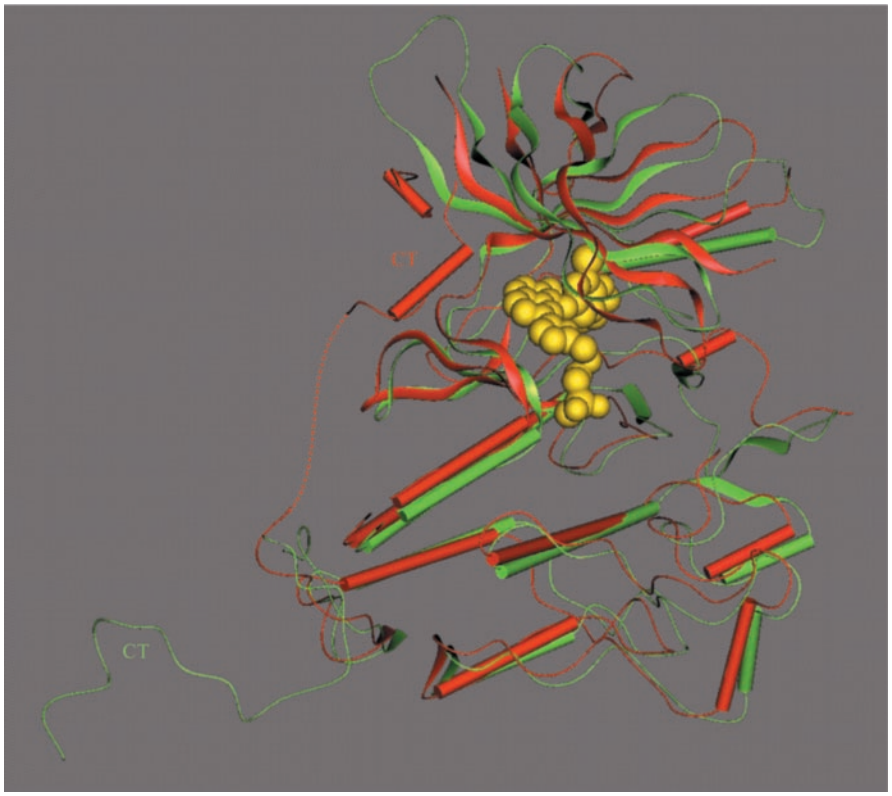

Fig. 5. Overlay of EGFR in the GW572016 and OSI-774 complexes. EGFR in the GW572016 and OSI-774 structures is shown as *red* and *green ribbons*, respectively. GW572016 is shown as a *yellow space-filling model*. The two proteins were overlaid based on residues in the COOH-terminal domain of the kinase. The COOH-terminal tail in both structures is *CT*. Disordered residues in the COOH-terminal tail of EGFR are indicated by a *dashed line*. The figure was prepared using QUANTA (Accelrys).

structures of inactive Src and Hck. Eight residues in the middle of the activation loop are disordered (844 to 851). The DFG motif of kinases is part of the A-loop and is involved in coordinating ATP. The side chains of Asp831 and Phe832 of the DFG motif form part of the expanded back pocket in GW572016/EGFR. Unlike apo and OSI-774/EGFR, residues 834 to 838 form a short helical segment that packs against the shifted C helix.

Finally, the quinazoline rings of OSI-774 and GW572016 hydrogen

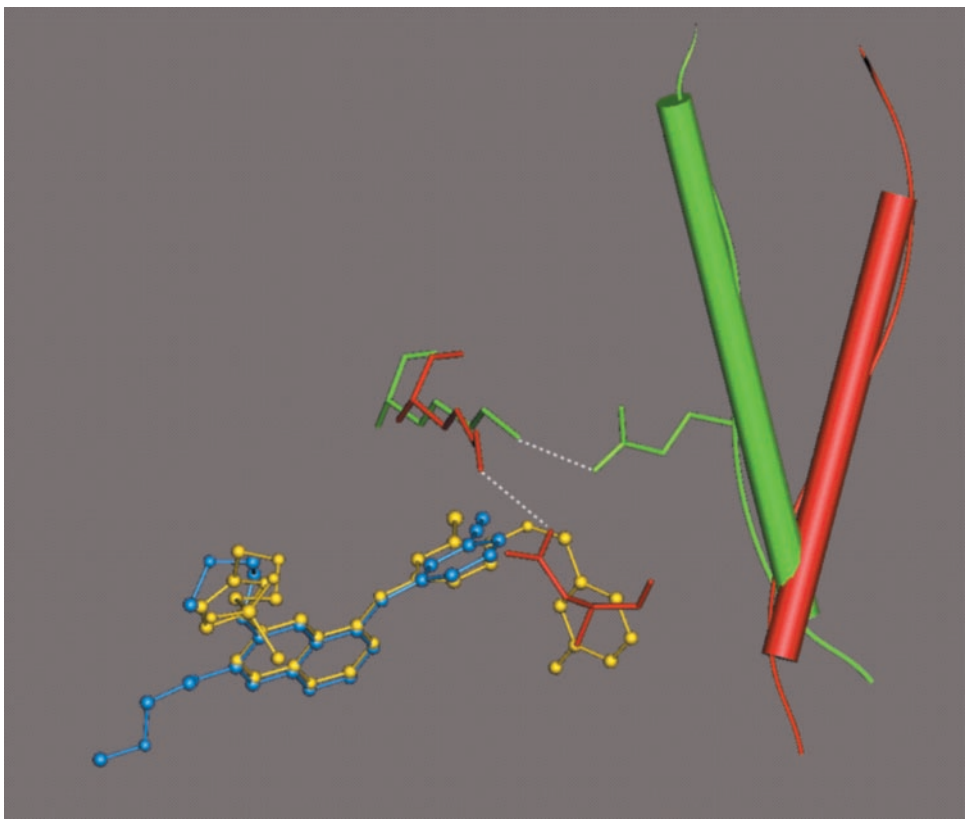

Fig. 6. Difference in C helix position in the GW572016 and OSI-774 EGFR structures. GW572016 and OSI-774 are shown as *yellow* and *blue ball* and *stick figures*, respectively. The C helix in the GW572016 and OSI-774 structures is shown as *red* and *green cylinders*, respectively. The hydrogen bonds between Lys721 and Glu738 in the OSI-774 structure and Lys721 and Asp831 in the GW572016 structure are indicated by *dashed lines*. The figure was prepared using QUANTA (Accelrys).

bond with EGFR differently. The quinazoline N1 of both compounds accepts a hydrogen bond from the main chain NH of Met769. However, N3 of GW572016 makes a water-mediated hydrogen bond to the side chain of Thr830 (Fig. 4). N3 of OSI-774 makes a water-mediated hydrogen bond with the side chain of Thr766. The side chain of Thr766 in GW572016/EGFR points away from the quinazoline and hydrogen bonds to the backbone carbonyl of Arg752. Interestingly, Blencke *et al.* (28) showed that mutation of Thr766 to methionine in EGFR leads to resistance to the 4-anilinoquinazoline PD153035. PD153035, like OSI-774, has a small 4-aniline substituent and is predicted to share a similar binding mode. This mutation may not affect inhibition by compounds that bind like GW572016.

It is important to note that the structures for GW572016/EGFR and OSI-774/EGFR described above were derived from crystals obtained using different methods. The published OSI-774/EGFR structure was derived from apo-EGFR crystals that had been soaked with the inhibitor to obtain the bound complex (12). The GW572016/EGFR structure was derived from crystals created by cocrystallization of EGFR and inhibitor. Unfortunately, acceptable cocrystals could not be obtained by soaking GW572016 into the apo-EGFR crystal. This probably results from the inability of the bulky aniline substitution of the compound to form a complex with the small back pocket found in the active-like conformation of apo-EGFR. Nevertheless, we believe these technical differences do not contribute to the observed structural differences for three reasons: (1) the magnitude of the protein conformation differences exceeds the degree normally caused by different crystal packing interactions, (2) we have obtained quinazoline/EGFR structures for compounds with small aniline substitutions similar to OSI-774 by cocrystallization and find active-like conformations (data not shown), and (3) we have obtained compound/EGFR structures for several other compounds with bulky-aniline substitutions similar to GW572016, and all of these have had similar inactive-like conformations (data not shown).

DISCUSSION

Our results begin to establish a framework for understanding how ErbB receptor structure influences the biological activity of kinase inhibitors in clinical development. We have identified several novel relationships including connections between protein structure and inhibitor off-rate, protein structure and receptor selectivity, and protein structure and mechanism of receptor activation.

ErbB Structure and Inhibitor Off-Rate. Significant differences in the structure of EGFR bound to OSI-774 and GW572016 may explain the differences in their observed dissociation rates. OSI-774 and ZD-1839, which have small aniline substituents off the quinazoline ring, have relatively rapid off-rates. OSI-774/EGFR has a conformation that is virtually identical to apo-EGFR. Thus, the rapid off-rate may reflect the fact that the inhibitor binds and dissociates from an active form of the enzyme without requiring any major changes in protein conformation. GW572016, on the other hand, has a bulky aniline substituent that reaches deep into an opened back pocket. This back pocket, which is not apparent in apo or OSI-774/EGFR, results from a shift in the position of the C-helix. The COOH-terminal tail is also shifted to a position that partially blocks the opening of the inhibitor-binding site. It appears that dissociation of GW572016 may require a conformational change in EGFR. A slow protein conformational change may explain the slow dissociation rate of GW572016. Alternatively, the different structure of GW572016/EGFR may provide a very tight binding affinity that results in the slow-off rate, and a conformational change may not be involved in inhibitor dissociation.

Treatment of tumor cells with OSI-774, ZD-1839, and GW572016 results in down-regulation of tyrosine phosphorylation of ErbB receptors (4, 5, 7). The recovery of receptor tyrosine phosphorylation after down-regulation is a complex process that involves the regulation of receptor kinase activity through inhibitor concentration and dissociation, receptor activation, and autophosphorylation. The rate of recovery may also be affected by additional regulatory mechanisms such as receptor recycling, degradation, and resynthesis. Nevertheless, we have found that the rate recovery of receptor phosphorylation in tumor cells reflects the inhibitor off-rate observed in enzyme assays. We observed very little recovery of EGFR tyrosine phosphorylation 96 hours after removal of GW572016. Thus, the inhibitor off-rate may be an important factor that affects the duration of drug activity *in vivo*.

ErbB Structure and Inhibitor Selectivity. ZD-1839 and OSI-774 are potent inhibitors of EGFR but not ErbB-2, although ErbB-2 has a very similar catalytic domain (88% identical). GW572016 on the other hand inhibits both enzymes with similar potency. The GW572016/EGFR structure is very different from the OSI-774/EGFR structure. The magnitude of the difference suggests that the two inhibitors target different forms of the enzyme, active and inactive. The lack of inhibition of ErbB-2 by OSI-774 may reflect the inability of ErbB-2 to adopt an active-like conformation as seen in the apo and OSI-774/EGFR structures. Interestingly, we and others have found that purified ErbB-2 is not very active using ATP-Mg as a substrate. The enzyme is 15-fold more active using ATP-Mn (15). The presence of ATP-Mn in the active site of ErbB-2 may compensate for a catalytically inefficient structure that differs from apo-EGFR. If apo-ErbB-2 cannot achieve this active-like structure, then compounds similar to OSI-774 may not be able to bind with high affinity.

Our results suggest that ErbB receptor tertiary structure may be a key component of inhibitor selectivity. The enzyme assays that we and others have used to describe the EGFR/ErbB2 inhibitor selectivity used purified intracellular domains of the receptors (4, 15, 29). Thus, it is possible that inhibitor selectivity could be different *in vivo*. Experiments with tumor cell lines suggest that this is not the case. For example, OSI-774 effectively inhibits EGFR tyrosine phosphorylation and proliferation of EGFR overexpressing tumor lines (5). The compound is not effective, however, at blocking ErbB-2 tyrosine phosphorylation (29) or blocking proliferation of tumor cells that overexpress ErbB-2 (7). A selective ErbB-2 inhibitor, CP-654577, has been described recently (29). This compound is a 4-anilino-quinazoline with a bulky aniline substitution somewhat similar to GW572016. CP-654577 effectively blocks ErbB-2 tyrosine phosphorylation in intact cells but not epidermal growth factor-stimulated EGFR tyrosine phosphorylation. The dual inhibitor, GW572016, effectively blocks EGFR and ErbB-2 autophosphorylation in cells and inhibits the proliferation of tumor cell lines that overexpress either EGFR or ErbB-2 (7).

ErbB Structure and Receptor Activation. Unlike most receptor tyrosine kinases, autophosphorylation of the A-loop is not required for ErbB receptor catalytic activity (30, 31). A variety of evidence suggests that ligand-induced dimerization and subsequent conformational change trigger activity (reviewed in ref. 32). However, the nature of the conformational change is not understood.

The conformation of GW572016/EGFR is similar in many ways to the inactive conformations of Src and Hck (23–25). These enzymes are multidomain kinases that have NH_2-terminal SH2 and SH3 regulatory domains linked to the catalytic domain. Activity is regulated by phosphorylation of a specific tyrosine in the COOH-terminal tail. Intramolecular binding of the SH2 domain to this residue keeps the enzyme in the inactive state. This regulatory mechanism has been referred to as a switch–clamp–latch model. Conformational changes in the C helix and activation loop constitute the switch. The SH3 and SH2 domains act like a clamp, fixing the relative orientation of the

NH_2- and COOH-terminal lobes. The phosphorylated tyrosine in the COOH-terminal tail is considered the latch.

Activation of EGFR and other ErbB receptors may be similar to Src in some respects. If the apo-inactive enzyme has a conformation similar to GW572016/EGFR, then the C helix is in a position that is not competent for activity. The position of the COOH-terminal tail, which packs along the hinge, is positioned in such a way that it may act as a regulatory clamp. Dimerization induced by ligand binding may result in a shift that releases the COOH-terminal tail and allows the C-helix and A-loop to adopt an active conformation.

Conclusions. GW572016/EGFR is found in an inactive-like conformation. We do not know if the inhibitor binds to a pre-existing pool of EGFR that is already in this inactive state or if inhibitor binding induces a change to this conformation. cAbl bound to STI-571 (also known as Gleevec and Imatinib) also has an inactive-like conformation (33). Binding to inactive kinase conformations may provide some advantages for blocking biological activity through mechanisms related to the overall signal transduction process. Alternatively, binding to an inactive form of a kinase (or inducing this conformation) may simply provide an advantage by reducing the rate of inhibitor dissociation, allowing for prolonged effects in biological systems after inhibitor concentrations have dropped. In support of the latter mechanism, we have found that EGFR receptor autophosphorylation recovers very slowly in tumor cells after treatment with the slow-off rate inhibitor GW572016.

Our results have important implications for protein kinase drug discovery. GW572016 binds a form of EGFR that is distinct from the previously described structure of EGFR bound to another drug in clinical development, OSI-774. Thus, specific drugs may target different forms of the same enzyme. The selectivity of these drugs seems to be significantly affected by the tertiary structure of the receptor target. Thus, the primary amino acid sequence of the kinase ATP binding site may not be a very good predictor of selectivity. The slow off-rate, bound EGFR structure, and dual ErbB1 and Erb2 inhibition profile differentiate GW572016 from the other clinical agents tested.

ACKNOWLEDGMENTS

Use of the IMCA-CAT beamline 17-ID at the Advanced Photon Source was supported by the members of the Industrial Macromolecular Crystallography Association through a contract with Illinois Institute of Technology. Use of the Advanced Photon Source was supported by the United States Department of Energy, Office of Science, Office of Basic Energy Sciences, under Contract No. W-31–109-Eng-38. We thank Jon Williams, Wendy White, Craig Wagner, and Erin Chaney for intact protein LC/MS of inhibitor-treated EGFR samples. We thank Dr. Gary Smith and Dr. Thomas Meek for critically reading this manuscript.

REFERENCES

1. Olayioye, MA, Neve, RM, Lane, HA, Hynes, NE. The ErbB signaling network: receptor heterodimerization in development and cancer. EMBO J. 2000;19:3159–67.
2. Arteaga CL. ErbB-targeted therapeutic approaches in human cancer. Experimental Cell Research 2003;284:122–30.
3. Fry DW. Mechanism of action of erbB tyrosine kinase inhibitors. Experimental Cell Research 2003;284:131–9.
4. Wakeling AE, Guy SP, Woodburn JR, et al. ZD 1839 (Iressa): An orally active inhibitor of epidermal growth factor signaling with potential for cancer therapy. Cancer Res 2002;62:5749–54.
5. Moyer JD, Barbacci EG, Iwata KK, et al. Induction of apoptosis and cell cycle arrest by CP-358,774, an inhibitor of epidermal growth factor receptor tyrosine kinase. Cancer Res 1997;57:4838–48.
6. Carter, MC, Cockerill, GS, Guntrip, SB, Lackey, KE, Smith, KJ. Bicyclic heteroaromatic compounds (quinazolinamines and analogs) useful as protein tyrosine kinase inhibitors. PCT Int. Appl. WO9935146, Glaxo Wellcome, 1999.
7. Rusnak DW, Lackey K, Affleck K, et al. The effects of the novel, reversible epidermal growth factor receptor/ErbB-2 tyrosine kinase inhibitor, GW572016, on the growth of human normal and tumor-derived cell lines in vitro and in vivo. Mol Cancer Ther 2001;1:85–94.
8. Smaill JB, Rewcastle GW, Loo JA, et al. Tyrosine kinase inhibitors. 17. Irreversible inhibitors of the epidermal growth factor receptor: 4-(phenylamino)quinazoline- and 4-(phenylamino)pyrido[3,2-d]pyrimidine-6-acrylamides bearing additional solubilizing functions J Med Chem 2000;43:1380–97.
9. Cockerill S, Stubberfield C, Stables J, et al. Indazolylamino quinazolines and pyridopyrimidines as inhibitors of the EGFR and c-ErbB-2. Bioorg Med. Chem Lett 2001;11:1401–5.
10. Gaul MD, Guo Y, Affleck K, et al. Discovery and biological evaluation of potent dual ErbB-2/EGFR tyrosine kinase inhibitors: 6-thiazolylquinazolines. Bioorg Med Chem Lett 2003;13:637–40.
11. Rusnak DW, Affleck K, Cockerill SG, et al. The characterization of novel dual ErbB-2/EGFR, tyrosine kinase inhibitors: potential therapy for cancer. Cancer Res 2001;61:7196–203.
12. Stamos J, Sliwkowski MX, Eigenbrot C. Structure of the EGF receptor kinase domain alone and in complex with a 4-anilinoquinazoline inhibitor. J Biol Chem 2002;277:46265–72.
13. Arnold, L, Schnur, R. Alkynyl and azido-substitutted 4-anilino-quinazoline derivatives are potent inhibitors of the erbB family of oncogenic and proto-oncogenic protein tyrosine kinase(s), useful for treating hyper-proliferative disorders. US Patent 5,747498. Pfizer, Inc. 1998.
14. Gibson KH. Quinazoline Derivatives. US Patent 5,770,599. Zeneca Limited, 1998.
15. Brignola PS, Lackey K, Kadwell SH, et al. Comparison of the biochemical and kinetic properties of the type 1 receptor tyrosine kinase intracellular domains. Demonstration of differential sensitivity to kinase inhibitors. J Biol Chem 2002;277:1576–85.
16. Copeland RA. Tight binding inhibitors. In: Enzymes. A practical introduction to structure, mechanism and data analysis. Second Edition. New York: Wiley-VCH; 2000. pp. 305–17.
17. Morrison JF, Walsh CT. The behavior and significance of slow-binding enzyme inhibitors. In: Meister, A. editor. Advances in Enzymology. New York: John Wiley and Sons; 1998. pp. 201–301.
18. Otwinowski Z, Minor W. Processing of X-ray diffraction data collected in oscillation mode. Methods Enzymol 1997;276:307–26.
19. Brunger AT, Adams PD, Clore GM. Crystallography & NMR system: A new software suite for macromolecular structure determination. Acta Crystallogr D Biol Crystallogr 1998;54:905–21.
20. Fry DW, Bridges AJ, Denny WA, et al. Specific, irreversible inactivation of the epidermal growth factor receptor and erbB2 by a new class of tyrosine kinase inhibitor. Proc Natl Acad Sci USA 1998;95:12022–7.
21. Modjtahedi H, Affleck K, Stubberfield C, Dean C. EGFR blockade by tyrosine kinase inhibitor or monoclonal antibody inhibits growth, directs terminal differentiation and induces apoptosis in the human squamous cell carcinoma HN5. Int J Oncol 1998;13:335–42.
22. Shewchuk L, Hassell A, Wisely B, et al. Binding mode of the 4-anilinoquinazoline class of protein kinase inhibitor: x-ray crystallographic studies of 4-anilinoquinazolines bound to cyclin-dependent kinase 2 and p38 kinase. J Med Chem 2000;43:133–8.
23. Sicheri F, Moarefi I, Kuriyan J. Crystal structure of the Src family tyrosine kinase Hck. Nature 1997;385:602–9.
24. Xu W, Harrison SC, Eck M. Three-dimensional structure of the tyrosine kinase c-Src. Nature 1997;385:595–601.
25. Williams JC, Weijland A, Gonfloni S, et al. The 2.35 Å crystal structure of the inactivated form of chicken src: a dynamic molecule with multiple regulatory interactions. J Mol Biol 1997;274:757–75.
26. Johnson LN, Noble MEM, Owen DJ. Active and inactive protein kinases: structural basis for regulation. Cell 1996;85:149–58.
27. Hubbard SR, Mohammadi M, Schlessinger J. Autoregulatory mechanisms in protein-tyrosine kinases. J Biol Chem 1998;273:11987–90.
28. Blencke S, Ulrich A, Daub H. Mutation of threonine 766 in the epidermal growth factor receptor reveals a hotspot for resistance formation against selective tyrosine kinase inhibitors. J Biol Chem 2003;278:15435–40.
29. Barbacci EG, Pustilnik LR, Rossi AMK, et al. The biological and biochemical effects of CP-654577, a selective erbB2 kinase inhibitor, on human breast cancer cells. Cancer Res 2003;63:4450–9.
30. Cadena DL, Chan C, Gill GN. The intracellular tyrosine kinase domain of the epidermal growth factor receptor undergoes a conformational change upon autophosphorylation. J Biol Chem 1994;269:260–5.
31. Tice DA, Biscardi JS, Nickles AL, Parsons SJ. Mechanism of biological synergy between cellular Src and epidermal growth factor receptor. Proc Natl Acad Sci USA 1999;96:1415–20.
32. Jorissen RN, Walker F, Pouliot N, Garrett TPJ, Ward CW, Burgess AW. Epidermal growth factor receptor: mechanisms of activation and signaling. Experimental Cell Research 2003;284:31–53.
33. Schindler T, Bornmann W, Pellicena P, Miller WT, Clarkson B, Kuriyan J. Structural mechanism for STI-571 inhibition of abelson tyrosine kinase. Science 2000;289:1938–42.

A Unique Structure for Epidermal Growth Factor Receptor Bound to GW572016 (Lapatinib): Relationships among Protein Conformation, Inhibitor Off-Rate, and Receptor Activity in Tumor Cells

Edgar R. Wood, Anne T. Truesdale, Octerloney B. McDonald, et al.

Cancer Res 2004;64:6652-6659.